

A Microfabricated Flow Controller for Refrigerant Expansion

David Yashar, Piotr A. Domanski, and Don L. DeVoe

Abstract—A flow controller for refrigerant expansion is reported. Devices are fabricated using a micromolding technique that is developed for thick nickel electrodeposition. The device consists of a short-tube restrictor with an integrated normally open valve, which, when actuated, presents a controllable blockage into the flow passage to obstruct the flow. Fabricated devices are evaluated with compressed air, with up to 22% reduction in mass flow rate at maximum actuation of the restrictor. The devices are also evaluated in an R134a vapor compression system of 1.5–2 kW, with the ability to control mass flow that is found to be greatly influenced by the vapor compression cycle's operational parameters. After the inlet pressure, the level of subcooling proved to be the most important parameter. For a cycle operating between 29 °C and 4 °C, saturation temperatures in the condenser and evaporator, respectively, actuation of the device reduced the refrigerant mass flow rate by 3.5% with 0.6 °C subcooling and up to 10.8% with 5 °C subcooling. [2006-0216]

Index Terms—Microfabricated valve, refrigerant expansion, SU-8.

I. INTRODUCTION

THE VAPOR compression cycle is commonly used to move thermal energy from a low-temperature reservoir to a high-temperature reservoir. Operation of the cycle requires that a refrigerant, flowing in a loop, undergoes four distinct processes: 1) compression; 2) condensation; 3) expansion; and 4) evaporation. Refrigerant expansion is described: As the process by which high pressure nearly saturated liquid refrigerant undergoes, a rapid reduction in pressure and partially (generally in the range of 15%–25% by mass) changes to vapor phase. This is generally accomplished by passing the refrigerant through some restrictive flow-metering device or passage.

Most small vapor compression systems use simple fixed-area flow restrictors as their expansion device. The simple design and low cost make them well suited for many applications. A major disadvantage of these devices is that they must be designed for a unique operating condition. Therefore, a system with a fixed-area expansion device loses efficiency when operating away from its design point, which routinely occurs through changes in the heating or cooling load, or in response

to a refrigerant leak. Improved operational efficiency can be realized if the expansion device has the ability to control the mass flow rate of the refrigerant, so that the demands of the application are aptly met, as this is the case with thermostatic expansion valves (TXVs); however, the expected improvement in system efficiency must be able to offset the higher cost of the TXV. If variable restriction devices could be produced at a low cost, then they would become economically viable in small systems as main expansion devices. Automotive air conditioning systems, for example, could employ such devices to improve their operational efficiency, ultimately translating to an improvement in fuel economy. Furthermore, they may be employed to control the flow through individual circuits of larger heat exchangers as components of smart refrigerant distributors [1].

Fabrication technologies that are developed for microelectromechanical systems (MEMS) processes have been widely explored as a means to develop fluidic valves. A silicon boss-and-valve seat type valve that is developed by Henning *et al.* [2], [3] has been demonstrated as a refrigerant expansion control device operating with mass flow rates of up to 3 g/s and differential pressures of up to 1 MPa. This device was fabricated using wet bulk silicon etching and relied on thermal expansion of an enclosed liquid to seal a valve seat with a membrane. Williams *et al.* developed a microvalve for which refrigerant expansion is named as a possible application [4], [5]. The valve was made from a three-layer stack of silicon, with valve operation based on thermal actuation of a sliding plate, which alters the dimensions of an orifice.

One aspect that must be considered when evaluating any valve that is developed for refrigerant expansion control is the minimum open area passage through the device. Vapor compression systems are constructed from metallic components, which are assembled through soldering and brazing; therefore, a certain level of particulate entrainment is expected within the refrigerant. If the flow of refrigerant is routed through a passage consisting of tight turns and small openings, it may be difficult to pass particles that are entrained in the refrigerant. Thus, it is desirable to ensure that the fluid passage is capable of passing entrained particles with ease. The present device meets this requirement by using a straight channel that is approximately 1000 μm wide by 500 μm tall, with no tight turns or small openings within the flow passage.

II. DEVICE FABRICATION

The basic concept of the refrigerant expansion device that is described here is rather simple. A fixed-area flow restrictor

Manuscript received October 3, 2006; revised February 7, 2007. Subject Editor Y. Zohar.

D. Yashar and P. A. Domanski are with the HVAC&R Equipment Performance Group, National Institute of Standards and Technology, Gaithersburg, MD 20899 USA (e-mail: dyashar@nist.gov).

D. L. DeVoe is with the Department of Mechanical Engineering, University of Maryland, College Park, MD 20742 USA.

Color versions of one or more of the figures in this paper are available online at <http://ieeexplore.ieee.org>.

Digital Object Identifier 10.1109/JMEMS.2007.900882

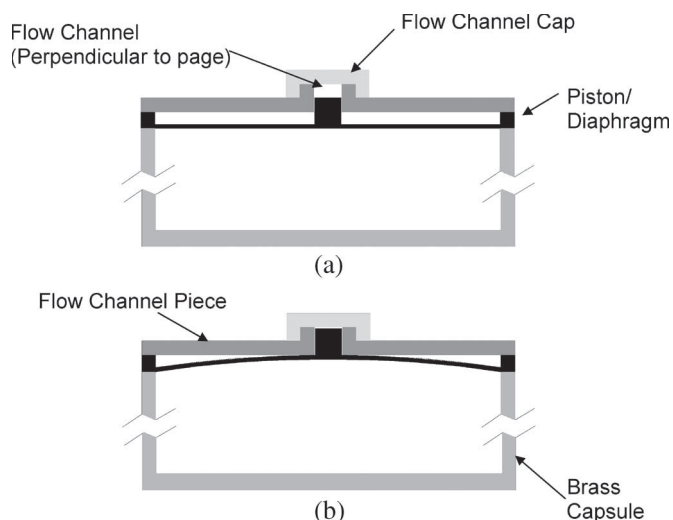


Fig. 1. Cross-sectional diagram of an assembled refrigerant expansion device in its (a) zero-power and (b) fully actuated positions.

is combined with a microfabricated actuator that is capable of controlling the degree of obstruction within the flow path. When the device is in a zero-power state, the flow passage is similar in nature to a common short-tube restrictor. As power is applied to the actuator, the flow passage becomes increasingly blocked by an obstruction that is fixed to one of the boundaries, thereby increasing the resistance and reducing the flow rate. Schematic drawings of the device in actuated and unactuated modes are shown in Fig. 1(a) and (b), respectively.

Each component of the device was fabricated by electrodeposition of metal into an array of microfabricated molds. The molds were fabricated using SU-8 formulation 2100 negative photoresist, and nickel was employed as the structural material. The device was fabricated in three discrete pieces, as labeled in Fig. 1, namely: 1) a diaphragm/piston section; 2) a flow channel section; and 3) a flow channel cap. The diaphragm/piston section comprises a 150- μm -thick circular membrane with a 1-mm-tall 950- μm -diameter cylindrical piston that is located at its center and a ring on its perimeter for mechanical stability. The flow channel section consists of a 500- μm -thick nickel plate with a 1-mm-diameter hole at the center, which mates with the piston. Two 500- μm -tall vertical walls that are separated by a 1-mm gap are connected to one side of the plate and positioned such that they lie on either side of the hole. These walls and the portion of the plate that lies between them make up the bottom and sides of the flow channel. The channel extends a short distance beyond the periphery of the plate, so that connections to external fluidic conduits may be made. The flow channel cap consists of a 500- μm -thick nickel film, which spans the length of the flow channel and includes a wall on either side to provide enhanced sealing of the channel.

The micromolded stack is mounted on top of a brass capsule whose 2.1-mL volume was filled with polyalkylene glycol (PAG). An electric resistance heating element and a thermocouple were secured within this reservoir. The device is controlled by regulating heat addition to the PAG through the heating element. In response to a small amount of heat addition, the

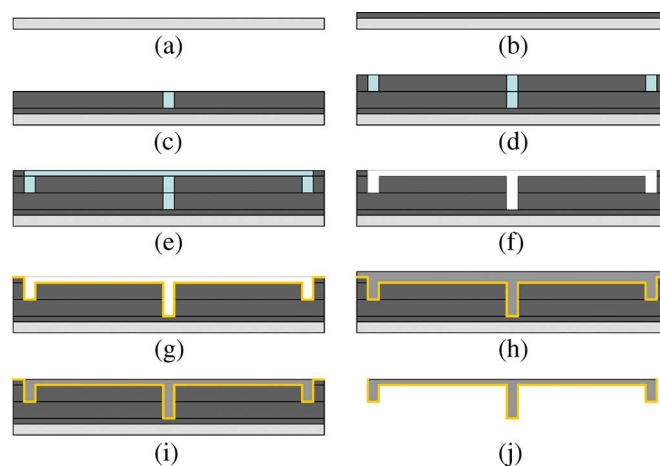


Fig. 2. Fabrication sequence for piston/diaphragm section.

temperature of the PAG increases, which decreases its density and flexes the membrane outward, forcing the piston into the flow path, thereby restricting the flow.

The process flow that is used to fabricate the piston/diaphragm section is outlined in Fig. 2. Similar process flows were employed for the other sections. Beginning with a cleaned substrate [Fig. 2(a)], a thin layer of SU-8 is deposited, soft baked, and flood exposed over the entire area [Fig. 2(b)]. This layer is necessary to prevent the final device from contacting the substrate. Next, a 500- μm layer of SU-8 is spun on top, soft baked, and patterned with the negative image of the piston [Fig. 2(c)].

There are many challenges in the construction of SU-8 molds that are greater than 1 mm thick, as required for the expansion device design. The most difficult obstacle is the development of large residual stresses [6], which often cause thick SU-8 to buckle, shatter, or lose adhesion to the substrate. Furthermore, the magnitude of this stress becomes greater as SU-8 is deposited in thicker and thicker layers [7]. The bulk of the stress in SU-8 is generated during the development stage of processing. This observation was determined by examining the curl that is induced in the substrates upon immersion in the developer solution of propylene glycol methyl ether acetate (PGMEA). In order to successfully develop SU-8 films that are thicker than 1 mm, a 900- μm -thick 10-cm-diameter silicon wafer was employed as the substrate since thinner wafers were found to either bow in excess of 1 cm or shatter when immersed in PGMEA.

Thick SU-8 layers were deposited in 500- μm -thick increments. Each 500- μm layer was formed by spinning on a 250- μm layer of SU-8 at 1000 r/min, soft baking for 1 h at 95 $^{\circ}\text{C}$, and repeating the process with another 250- μm layer. After spin coating each 500- μm -thick layer, a thick edge bead was formed at the wafer periphery. A photolithography mask was used to expose only the outer edge of the wafer, forming an SU-8 dish that is defined by the polymerized edge bead. SU-8 formulation 2025 was next dispensed into the dish and leveled using the edge of a glass plate. The SU-8 then underwent an extended low-temperature soft bake at 75 $^{\circ}\text{C}$ for 18–22 h to drive off the solvents. The resulting unpolymerized SU-8 thick

film was sufficiently flat for contact photolithography to be performed. Each 500- μm layer was given a UV exposure dose of 5.4 J/cm².

In Fig. 2(d), another 500- μm -thick layer of SU-8 is deposited, soft baked, and patterned with the negative image of the piston and the stability ring. In Fig. 2(e), a 150- μm -thick layer of SU-8 was spun on top of the stack at 1850 r/min, soft baked for 35 min at 95 °C, and patterned with the negative image of the diaphragm using an exposure dose of 3.3 J/cm².

Once all layers of SU-8 were deposited and exposed, the entire stack was given a postexposure bake for 19 h at 75 °C. The wafer was submerged in PGMEA [Fig. 2(f)] for development. With the resulting overall thickness, the development process took approximately 80 min with agitation and periodic changes of the developer solution. All SU-8 layers were developed together to minimize interfacial stress between layers. The structure remaining after development is the mold that was used to produce the piston/diaphragm section of the device. Next, the entire substrate was coated with a 480-nm-thick layer of gold by sputtering [Fig. 2(g)]. The metallic plating base was deposited on top of the SU-8 molds, rather than underneath them, because the adhesion between SU-8 and sputtered gold is not as great as that between SU-8 and silicon. The molds were then filled with Ni via DC electrodeposition [Fig. 2(h)] with a current density of 12.7 mA/cm². The electrodeposition process took approximately 90 h until the Ni grew sufficiently beyond the mold thickness. In Fig. 2(i), the Ni was ground and polished to the desired thickness.

Finally, the pieces were removed from the SU-8 molds using thermal shock [Fig. 2(j)]. Removing cured SU-8 from the micromolded metal pieces is a substantial challenge, and numerous chemical and plasma methods for SU-8 removal have been explored [8], [9]. However, with features as large and mechanically rigid as the ones that are employed for the refrigerant expansion device, a much simpler method was developed. Since the SU-8 molding was near its maximum stress limit, placing the wafer on top of a 500 °C hot plate for 5–10 s caused the rigid SU-8 to shatter, leaving the nickel micromolded pieces and the silicon wafer intact.

After solvent cleaning, the Ni pieces were joined to each other and to the brass capsule by a bake-soldering method. Since some of the features on the micromolded pieces inherently make good conduits for solder to flow, a method was devised to ensure that no solder neared these features. Solder was ground up into small chards and mixed with soldering flux. This mixture was then painted into the crevices between adjoining surfaces using a thin wire, and the assembled stack of pieces was placed onto a hot plate until it could be visually verified that the solder chards were melted. Once the prototype was assembled, it was connected to a pair of copper tubes, and its performance was benchmarked.

III. EXPERIMENTAL RESULT AND DISCUSSION

A. Fabrication Results

It was observed that the openings in the SU-8 molds were slightly smaller than intended. This is because of the number of

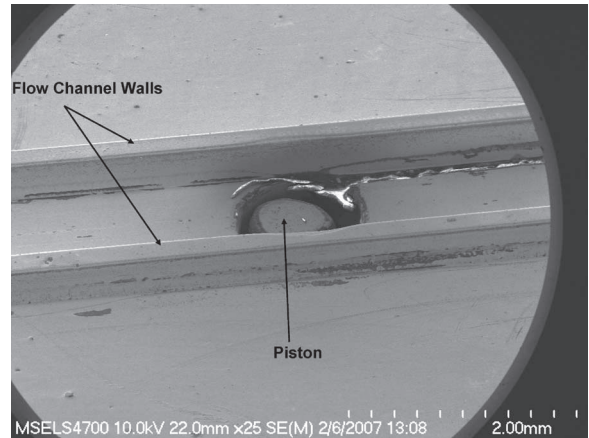


Fig. 3. Electron micrograph of a flow controller without flow channel cap.

exposure steps and the overall thickness of the SU-8. Misalignment and scattering both result in dark fields receiving some UV radiation. In addition, there is some difficulty removing undeveloped SU-8 from the bottom of a 1000⁺- μm deep trench, which correspond to features at the top of the metallic objects; this ultimately results in rounded edges. In general, this process resulted in Ni positive features (posts and walls) that were slightly thinner than the target and in negative features (holes and trenches) that were slightly wider. As an example, the intended geometry of the piston was to be that of a cylinder that is 1000 μm tall, with a diameter of 950 μm . For the tested device, the height of the piston was 993 μm , with the diameter at the top of the post measuring 900 and 913 μm along two perpendicular chords. Detailed characterization maps and tables can be found in [10].

An electron micrograph depicting a partially assembled device is shown in Fig. 3. Note that a small clearance exists between the nominal position of the piston and the flow channel floor due to the effects that were discussed previously. Some clearance is necessary to ensure that the device will function, while excessive clearance will reduce the amount of control that the piston can exert on the fluid passing through the channel.

1) *Compressed Air Testing*: Initial testing of a fabricated prototype was performed to demonstrate its ability to control the flow of compressed air. Before experimental testing, theoretical performance of the refrigerant expansion device was computed using a commercially available computational fluid dynamics (CFD) software package. Numerical simulations were performed to calculate the mass, momentum, and energy equations within a domain that is representative of the valve's flow channel. Each data point was acquired by a simulation over a geometrical mesh that is representative of the device at a specified level of piston actuation. Air was modeled as the fluid passing through the device, with constant inlet boundary conditions of 300 K and 316 kPa, an exit pressure of 202 kPa, and adiabatic walls. These conditions were chosen since they can be easily replicated with laboratory measurements. The CFD analysis determined the mass flow rate of air as a function of piston displacement. Simulations were performed, assuming a flow channel of rectangular cross section with a width of 1000 μm and a height of 500 μm , which are the designed

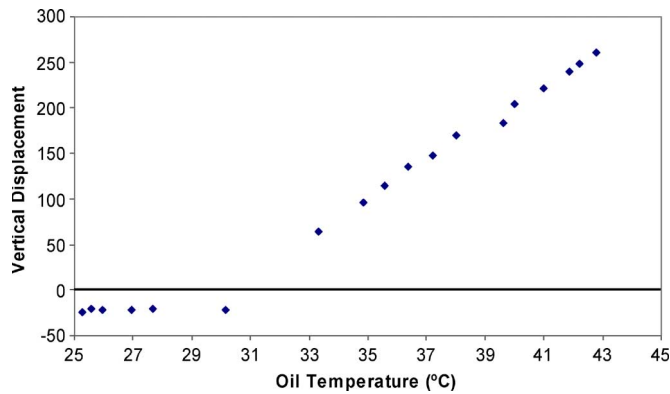


Fig. 4. Measured relationship between reservoir temperature and piston extension, with displacement relative to channel floor.

feature specifications of the device. To simplify the simulation, the piston was assumed to fully occlude the width of the flow path.

Initial testing of a fabricated device was performed to evaluate its ability to control flow using a test apparatus consisting of a compressed air source, a needle valve to control the upstream pressure, another needle valve to control the downstream pressure, and an inverted graduated cylinder in a water bath for air collection. The objective was to measure the flow rate of air through the prototype for various actuation levels while holding the inlet and exit pressures constant. The supply and back pressures were adjusted manually to be as close as possible to the inlet and outlet boundary conditions that are used for CFD analysis of 316 and 202 kPa, respectively. In all cases, the supply pressure was between 312.5 and 317.6 kPa, and the back pressure was between 200 and 204 kPa. For each measurement, the power input to the device was held constant, while the needle valves were adjusted, so that the upstream and downstream pressures matched the prescribed conditions. Once they were met, the air passing through the device was collected over a measured period of time and used to calculate the mass flow rate.

Prior to taking the air flow rate measurements, a relationship was derived to calculate the piston displacement based on the thermophysical properties of the PAG, the capsule geometry, and the measured PAG temperature. However, the actual relationship between these parameters could only be determined through destructive testing by cutting the flow channel cap from the device and measuring the piston displacement over a range of oil temperatures. Thus, while the theoretical relationship was used as a tool to aid in initial interpretation of experimental measurements, the device was dissected once testing was completed, and measurements were taken to determine the real relationship between the oil temperature and the piston extension. This relationship, as shown in Fig. 4, was subsequently used to fit all of the measured data. As evident from this plot, the device did not exhibit any displacement at low temperature. This behavior is likely due to the presence of a small void in the capsule that must collapse before significant pressure change is realized.

The results from the CFD and experimental measurements for compressed air flow are shown in Fig. 5. Two observations

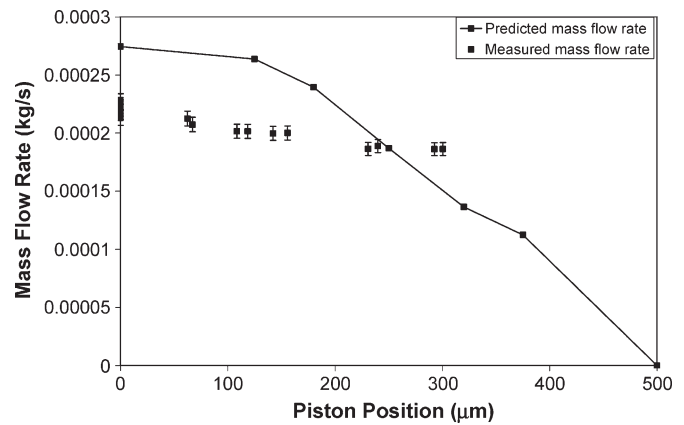


Fig. 5. CFD predicted and experimentally measured (95% confidence) compressed air flow rates through the expansion device relative to piston actuation height.

from this figure should be noted. First, the measured air flow rate at zero actuation is 17% less than the simulated value. This discrepancy is primarily due to differences between the simulated and experimental device dimensions. While the channel width of the experimental device was 75 μm wider than the simulated, the measured channel height was 100 μm smaller, resulting in an overall cross-sectional area that is 14% lower than that of the simulated geometry, leading to the lower experimental air flow rate in the fully open (zero piston displacement) device.

A second observation is that, while the slope of the simulated data changes in the vicinity of 150- μm piston displacement, the slope of the experimental data does not change significantly over the range of data. Considering the numerical simulation results, the first two data points, which correspond to zero actuation and a piston height of 125 μm , show a flow regime that is subsonic throughout the entire domain. A transition from entirely subsonic to choked flow occurs somewhere between the 125- μm data point and the 180- μm data point. Here, the passage becomes small enough to accelerate the flow to Mach 1 between the piston top and the upper channel wall. For any level of actuation beyond this transition point, the flow rate is directly related to the cross-sectional flow area. In contrast, the experimental data does not reveal the flow regime transition. This difference is believed to result from incomplete blocking of the microchannel width in the experimental device. While the simulation assumed a piston diameter that is matched to the channel width, the experimental device was fabricated with a measured piston diameter that is 168 μm smaller than the channel width. The geometry that was employed in the simulation was chosen to simplify the numerical analysis while providing substantive information about the general relationship between piston displacement and fluid flow through the constriction. As a result of the gap between the piston and channel walls, the flow does not become choked over the 300- μm piston displacement range that is considered in the experimental study. Thus, the measured mass flow rate data follow a similar trend as the CFD simulations at low piston displacements. Overall, the measured mass flow rate was reduced by 22%, as the piston was pushed to its maximum distance of 300 μm

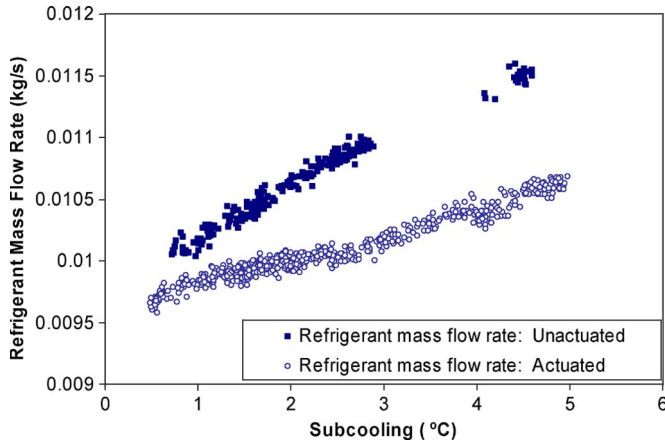


Fig. 6. Steady-state refrigerant mass flow rate for two levels of actuation.

into the flow channel. Higher piston displacements were not attempted to avoid the possibility of damaging the actuator membrane.

2) *Testing in a Vapor Compression System:* Tests were also performed to measure the mass flow rate of refrigerant passing through the microfabricated device in an R134a vapor compression laboratory system of 1.5–2 kW. The performance was first evaluated at steady state with a fixed set of device inlet and exit pressures. The condenser exit pressure was held constant at 750 kPa ($T_{\text{sat}} = 29^\circ\text{C}$), and the evaporator inlet pressure was 338 kPa ($T_{\text{sat}} = 4^\circ\text{C}$), while the level of liquid line subcooling was varied. Two levels of actuation were used to characterize the operation of the device, corresponding to high and low levels of interaction between the piston and the flashing refrigerant. For the low actuation level, the piston was not engaged with the flow, effectively making the device perform as a short-tube restrictor. At the high level of actuation, the piston was elevated into the flow channel. Fig. 6 shows the results of these measurements.

It is interesting that the effect on the mass flow rate from actuating the device is strongly related to the level of subcooling. At low levels of subcooling, the effect is very small, showing, on average, 3.5% difference at 0.6°C subcooling. As the level of subcooling is increased, so is the impact of the device's actuation; at 5°C subcooling, there is a 10.8% difference in the refrigerant mass flow rate.

It has been observed through short-tube flow visualization experiments [11] that, as subcooling is increased, the transition point from liquid to two-phase flow moves further downstream within the short tube. Extending these observations to the work in this paper, it seems likely that this trend can be explained by the transition point from liquid to two-phase flow, being closer to the point of interaction with the piston, which would effectively make the transition less dependent on the level of subcooling. Further laboratory experimentation is necessary to evaluate this.

The system's dynamic response was also evaluated with a square-wave input that is applied to the electrothermal actuator. Three power levels were applied to the device, with progressively higher power each time, until the maximum output of the heater was reached. For the initial operation, the condenser

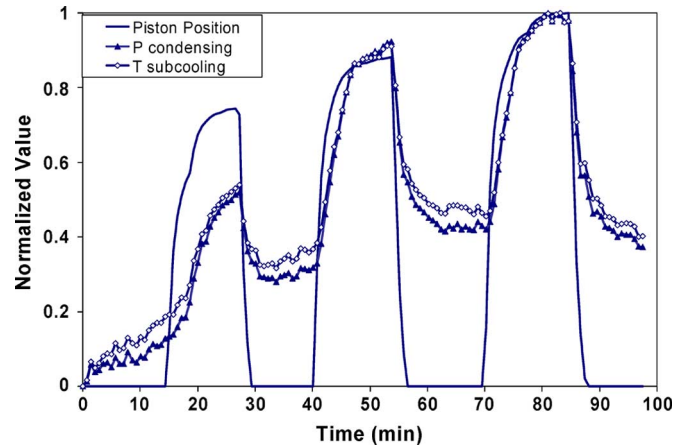


Fig. 7. Transient response of condensing pressure and subcooling to escalating square-wave input power.

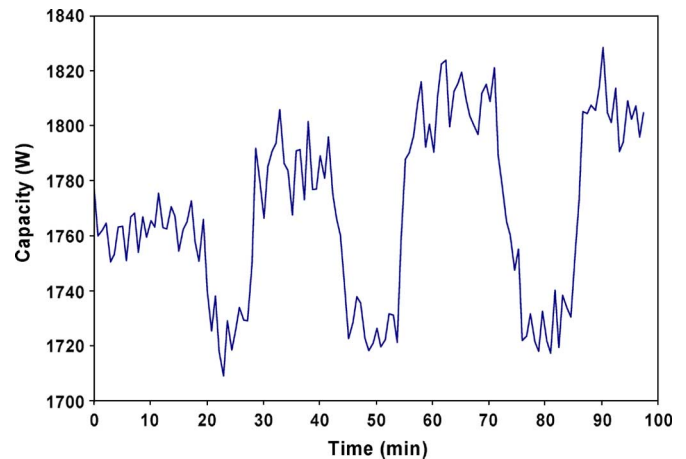


Fig. 8. Transient response of system capacity to escalating square-wave input power.

exit conditions were approximately 725 kPa with 4°C of subcooling.

Fig. 7 shows the transient response of the vapor compression system including inlet subcooling and inlet pressure as a function of piston position. Fig. 8 further reveals that the difference in system capacity between the unactuated device and the maximum input power level is only about 5%. There are a few factors that can help explain this limited response. One factor is that the piston was designed to have clearance inside the channel and therefore has a slightly smaller diameter than the width of the flow channel; thus, it does not completely block off this area. In addition, the heater that is used to input power to the device was slightly undersized and, consequently, was not capable of elevating the piston to the top of the flow channel. Combined, these two effects limited the maximum amount of flow channel blockage. Despite these limitations, the system capacity was shifted by approximately 100 W using a device input of only 2.75 W. Even for this preliminary study, the demonstrated performance may be sufficient modulation for some applications. Different operating conditions will, of course, produce different results.

Another factor is that the behavior of this device is, in general, similar to that of a short-tube restrictor, in which the flow rate is strongly influenced by the level of subcooling. When the device becomes more restrictive, the refrigerant migrates to the high-pressure portion of the system, which causes the condensing pressure and subcooling to both increase. With any type of flow-metering device, the pressure differential across the device is the driving potential for the flow (although, in the case of expansion in this configuration, the mass flow rate is unaffected by the low side pressure). Therefore, raising the condensing pressure will increase the flow potential. The subcooling, however, is not an obstacle for most other types of flow-controlling devices since the refrigerant is typically flashed at the exit plane of these devices. Due to the fact that the upstream pressure and subcooling both increase when the device is actuated, two driving potentials for the flow are increased, and the overall impact of the increased restriction is lessened.

IV. SUMMARY

The design, fabrication, and testing of a microfabricated refrigerant expansion device have been presented in this paper. A prototype of this device was constructed and demonstrated on both an air flow test bench and an R134a vapor compression system of 1.5–2 kW. Both steady-state and transient tests were performed. The steady-state tests showed that the level of flow control is strongly dependent on the refrigerant subcooling. The transient tests were performed to demonstrate the system's response to actuation of the device.

For the air flow measurements, it was demonstrated that this device could change the flow rate by approximately 22% under the given flow conditions with 300- μm piston elevation. However, the underlying physics of flow with liquid-to-vapor phase transition is vastly different from single-phase gaseous flow. With volatile refrigerant, the piston interaction will certainly impact, if not be the cause of, the onset of the liquid-to-vapor transition within the device. The data in this paper show that the flow through the device with some piston actuation is less sensitive to subcooling than the flow through the unactuated device. With zero piston actuation, the change in mass flow rate was 16.8%, as the subcooling was increased from 0.6 °C to 5.0 °C; with actuation, the change in mass flow rate was 9.1% over the same set of operating conditions. A possible explanation is that the location of the flow's liquid-to-vapor transition point is fixed by the piston, which would limit the subcooling's effect on the mass flow rate. Ultimately, introducing the piston changes the relationship between mass flow rate and subcooling. Therefore, data show that this device exerts much greater flow control at higher levels of subcooling. At 0.6 °C subcooling, the difference between the mass flow rates of the actuated and unactuated device is 3.5%; at 5 °C, this difference increases to 10.8%.

In order to develop this device to a usable standard within industry, a considerable amount of work must be done. Since this is the first pass at a new concept, a number of the auxiliary components and measurement techniques need to be redesigned to improve the performance of this device. In addition, the

results of the vapor compression system tests pose exploratory work that is related to refrigerant expansion within the complex flow geometry that is prescribed by this device.

ACKNOWLEDGMENT

The authors would like to thank Dr. D. Didion and Dr. M. Kedzierski of the HVAC&R Equipment Performance Group, National Institute of Standards and Technology (NIST), for their constructive criticism of this paper, and Dr. J. Bonevich of the Material Science and Engineering Laboratory, NIST, for his assistance and equipment use.

REFERENCES

- [1] W. V. Payne and P. Domanski, "Potential benefits of smart refrigerant distributors," Air-Conditioning and Refrigeration Technol. Inst., Arlington, VA, ARTI-21CR/605-200-50-01. [Online]. Available: <http://www.fire.nist.gov/bfrlpubs/build02/PDF/b02130.pdf>
- [2] A. K. Henning, "Microfluidic MEMS," in *Proc. IEEE Aerosp. Conf.*, 1998, pp. 471–486.
- [3] A. K. Henning, J. Fitch, D. Hopkins, L. Lilly, R. Faeth, E. Faeth, E. Falsken, and M. Zdeblick, "A thermopneumatically actuated microvalve for liquid expansion and proportional control," in *Proc. Transducers, Int. Solid State Sens. and Actuators Conf.*, 1997, pp. 825–828.
- [4] K. R. Williams, B. P. van Driehhuizen, D. P. Jaeggi, N. I. Maluf, E. N. Fuller, and R. J. Barron, "Microvalve with pressure equalization," U.S. Patent 6 523 560, Feb. 25, 2003.
- [5] K. R. Williams, N. I. Maluf, E. N. Fuller, R. J. Barron, D. P. Jaeggi, and B. P. van Driehhuizen, "A silicon microvalve for the proportional control of fluids," in *Proc. Dig. 10th Int. Conf. Solid-State Sens. and Actuators (Transducers)*, Sendai, Japan, Jun. 1999, pp. 1804–1807.
- [6] C. H. Lin, G. B. Lee, B. W. Chang, and G. L. Chang, "A new fabrication process for ultra-thick microfluidic microstructures utilizing SU-8 photoresists," *J. Micromech. Microeng.*, vol. 12, no. 5, pp. 590–597, Sep. 2002.
- [7] H. Lorenz, M. Despont, N. Fahrni, J. Brugger, P. Vettinger, and P. Renaud, "High-aspect-ratio, ultrathick, negative-tone near-UV photoresist and its applications for MEMS," *Sens. Actuators A, Phys.*, vol. 64, no. 1, pp. 33–39, Jan. 1998.
- [8] P. M. Dentinger, W. M. Clift, and S. H. Goods, "Removal of SU-8 photoresist for thick film applications," *Microelectron. Eng.*, vol. 61/62, pp. 993–1000, 2002.
- [9] C. H. Ho, K. P. Chin, C. R. Yang, H. M. Wu, and S. L. Chen, "Ultrathick SU-8 mold formation and removal, and its application to the fabrication of LIGA-like micromotors with embedded roots," *Sens. Actuators A, Phys.*, vol. 102, no. 1, pp. 130–138, Dec. 2002.
- [10] D. Yashar, "Design, measurements and performance predictions for a micromolded refrigerant expansion device," United States Dept. Commerce, Washington, DC. Rep. NISTIR 7372, Apr. 2006.
- [11] Y. Kim, "Two-phase flow of HCFC-22 and HFC-134a through short tube orifices," Ph.D. dissertation, Texas A&M Univ., College Station, TX, 1993.



David Yashar received the M.S. degree from the Air Conditioning Research Center, University of Illinois, Urbana-Champaign, in 1998, and the Ph.D. degree with a specialization in microelectromechanical systems from the University of Maryland, College Park, in 2006.

He is currently a Mechanical Engineer in the HVAC&R Equipment Performance Group, National Institute of Standards and Technology (NIST), Gaithersburg, MD. His work primarily focuses on developing innovative ideas that improve the efficiency, reliability, and intelligence of HVAC&R components and systems. His current research interests include sensor/actuator schemes, particle image velocimetry measurements, computational modeling, and genetic-algorithm-based methods to improve component efficiency.



Piotr A. Domanski received the Ph.D. degree from Catholic University of America, Washington, DC, for the modeling of vapor compression heat pumps in 1982.

He was later involved in studies related to ozone-safe alternative refrigerants. He is currently a Leader of the HVAC&R Equipment Performance Group, National Institute of Standards and Technology, Gaithersburg, MD. His current research focuses on novel ways and means that improve the efficiency and reliability of HVAC&R systems.

Dr. Domanski is a Regional Editor for the Americas for the *International Journal of Refrigeration*. He was the recipient of the Science and Technology Medal for the International Institute of Refrigeration and a Silver Medal from the U.S. Department of Commerce.



Don L. DeVoe received the Ph.D. degree in mechanical engineering with a specialization in microelectromechanical systems and piezoelectric microsystems from the University of California, Berkeley, in 1997.

He is currently an Associate Professor of mechanical engineering in the Department of Mechanical Engineering, University of Maryland, College Park, and a core faculty member of the Bioengineering Graduate Program. He is the holder of six U.S. patents in microsystems technology. His current research interests include microfluidic systems for

biomolecular analysis and interfacing with mass spectrometry.

Dr. DeVoe is a recipient of the Presidential Early Career Award for Scientists and Engineers from the National Science Foundation for advances in microsystems technology.